Radiation Measurements 195 (2026) 107699

Contents lists available at ScienceDirect

Radiation Measurements

journal homepage: www.elsevier.com/locate/radmeas

International intercomparison of passive radiation dosimetry in simulated lightning discharges using a high-voltage impulse generator

D. Štěpánová [a,b,*], J. Mikeš [c], V. Štěpán [b], I. Ambrožová [a], M. Bolzonella [e], M. Caresana [e], L. Garlati [e], M. Košťál [h], M. Krbal [d], M. Lužová [a,b], A. Mele [e], F. Trompier [f], M. Wiliński [g], O. Ploc [a]

[a] Department of Radiation Dosimetry, Nuclear Physics Institute of the Czech Academy of Sciences, Na Truhlářce 39/64, Prague, 18000, Czechia
[b] Czech Technical University in Prague, Faculty of Nuclear Sciences and Physical Engineering, Břehová 7, Prague, 11519, Czechia
[c] Czech Technical University in Prague, Faculty of Electrical Engineering, Technická 2, Prague, 16627, Czechia
[d] University of Technology, Faculty of Electrical Engineering and Communication, Technická 10, Brno, 61600, Czechia
[e] Politecnico di Milano, Department of Energy, Via Lambruschini 4a, Milan, 20156, Italy
[f] Authority for Nuclear Safety and Radiation Protection, Laboratory of Ionizing Radiation Dosimetry, Fontenay-aux-roses, 92262, France
[g] National Centre for Nuclear Research, Andrzeja Soltana 7, Otwock, 05-400, Poland
[h] Research Centre Řež s.r.o., Hlavní 130, Husinec Řež, 25068, Czechia

ARTICLE INFO

Keywords:
Lightning
Radiation
Passive detectors
High voltage impulse generator
Electric discharge

ABSTRACT

This work follows up on and expands previous studies dealing with the detection of ionizing radiation in the vertical field of an electric discharge generated between the electrode tip and a grounded plate electrode. The aim of the experiment was to measure the radiation dose in detail along the entire high voltage discharge covering 180° around the discharge axis at a radius of 1 m. The settings of the pulsed high voltage generator were the same as in the previous experiments: voltage amplitude 0.9 MV, waveform shape 1.2/50 μs, discharge energy 80 kJ and electrodes 1 m apart. In this experiment, the number of negative discharges was increased from 400 to 1000 pulses, for better statistics. Passive detectors were used to detect ionizing radiation in order to eliminate the influence of the electromagnetic field of the impulse generator and the discharge itself.

1. Introduction

The natural conditions associated with lightning discharges are difficult to predict and reproduce in a laboratory. It is impossible to simultaneously achieve the high voltage and high current typical of lightning, so phenomena related to lightning can only be studied using separate high-voltage and high-current impulse generators.

The generation of high-energy photon radiation in thunderstorm environments is generally attributed to bremsstrahlung emitted by energetic electrons accelerated in strong atmospheric electric fields. In natural conditions, these electrons may propagate over distances of hundreds of meter to several kilometer (Dwyer, 2008; Kovář et al., 2023). Such long acceleration paths provide sufficient air mass for efficient bremsstrahlung production, leading to the intense gamma-ray emission observed in phenomena such as terrestrial gamma-ray flashes (TGFs) and gamma-ray glows (GRGs).

In contrast, laboratory high-voltage discharges are characterized by acceleration lengths limited to at most a few meters. Under these conditions, the available interaction path in air is orders of magnitude shorter than in the atmosphere, which drastically reduces the bremsstrahlung yield. As a result, the photon component generated in laboratory discharges is expected to be much weaker and often close to the detection limits of passive dosimetry systems. This fundamental scaling difference provides a natural explanation for the relatively low absorbed doses measured in the present experiment.

To simulate a lightning discharge in laboratory conditions, high-voltage generators (HVG), most often Marx generator types, were used (Agafonov et al., 2013, 2017; Bassi et al., 2017; Dwyer et al., 2008; Nguyen et al., 2008; Rahman et al., 2008; Kochkin, 2014; Hettiarachchi et al., 2017b,a; Rahman et al., 2019). The range of basic generator setting parameters were: voltage amplitude 0.11–1.27 MV with an average value of 1 MV, electrode distance 0.1–1.74 m with an average range of 0.45–1.2 m, waveform 1.2/50 μs (impulse; lead time: 1.2 μs, half-fall time: 50 μs) and negative polarity for horizontal and vertical orientation of the discharge. A detailed overview of lightning discharge experiments on HVG is given in Tables 1 and 2.

The majority of the experiments described were devoted to the detection of photon and electron emissions generated by high-energy

* Corresponding author at: Department of Radiation Dosimetry, Nuclear Physics Institute of the Czech Academy of Sciences, Na Truhlářce 39/64, Prague, 18000, Czechia.
E-mail addresses: kyseldag@gmail.com (D. Štěpánová), mikes.jan@fel.cvut.cz (J. Mikeš).

https://doi.org/10.1016/j.radmeas.2026.107699
Received 2 February 2026; Received in revised form 4 April 2026; Accepted 10 April 2026
Available online 21 April 2026

Table 1
Overview of lightning discharge experiments in a laboratory environment (part 1).

Study	Nguyen et al. (2008)	Rahman et al. (2008)	Dwyer et al. (2008)	Agafonov et al. (2013)	Kochkin (2014)	
Generator type	Marx generator	Marx generator	Marx Generator	HVG	Marx generator	Marx generator
Voltage [MV]	0.85	1	1	1	1	1.27
Polarity	negative/positive	negative	negative/positive	not specified	positive	negative
Wave type [μs]	1.2/50	1.2/50	1.2/50	not specified	1.2/50	1.2/50
Electrode gap [m]	0.7–1.2	0.8	0.1–1.4	0.45 and 0.6	1	1–1.75
Electrode shape [–]	tips	rod with screw — hemisphere	spherical, rod and sphere, rod and plane	spherical	cones and cone–cone with belt with 75 sharp dots	cones
Electrode material [–]	aluminum	rod: brass, hemisphere: tungsten coating copper	small spheres: tungsten coating copper, large spheres: chromium coating copper, rod: brass, plane: not specified	not specified	cones: not specified, belt: aluminum	not specified
Electrode diameter [cm]	0.2	rod: 0.1, hemisphere: 6	spheres: 2–12, rod: 1, tip: 0.6	not specified	cone: not specified, belt: 55 × 10	not specified
Discharge orientation	horizontal	horizontal	vertical/horizontal	horizontal	vertical	vertical
Detectors	NaI(Tl) scintillator with PMT, $LaBr_3$(Ce) scintillator with PMT, BaF_2 scintillator with PMT	BaF_2 scintillator (2.2 × 4 × 4 cm) with PMT	NaI scintillator (7.6 × 7.6 cm) with PMT, plastic scintillator (36 × 25 × 1 cm) with PMT	CR-39 with PE radiator, CR-39 with ^{10}B radiator and plastic scintillator with POPOP	$LaBr_3$(Ce+) scintillator	$LaBr_3$(Ce+) scintillator
Distance of the detector from the discharge [m]	0.8 and more	1	0.5	1.5 (plastic scintillator), 0 (CR-39 on anode and cathode)	0.15–1.5	0.15-2.1
Detector shielding [–]	yes	yes	yes	only plastic scintillators	yes, only in some cases	yes, only in some cases
Shielding material	aluminum	steel, aluminum, polyethylene	aluminum	lead or aluminum	aluminum	aluminum
Shielding thickness [mm]	0.05	steel: 1, aluminum: 15, polyethylene: 15	3.2	lead: 100, aluminum: 0.01	0.55	0.55
Number of discharges [–]	5000	83	231	90 for each distance	951	3281 (over 3 years)
Gamma/X-ray detection [–]	yes	yes	yes	yes	yes	yes
Neutron detection [–]	not measured	not measured	not measured	yes (fast)	not measured	not measured

electrical discharges by HVG. Active detection systems, most commonly various types of scintillation detectors, were primarily employed for photon/electron measurements. To suppress electrical interference, detectors were typically enclosed within shielding composed of appropriate materials such as aluminum, lead or copper. Passive detectors were used only in Bassi et al. (2017), specifically LiF thermoluminescent detectors (TLDs) were chosen, representing a very widespread type of these detectors.

Only the experiments presented in Agafonov et al. (2013, 2017) dealt with the detection of the neutron component in the radiation field of HVG. To detect this radiation component, a plastic scintillation detector and a ^{3}He proportional detector with a paraffin moderator were used as representatives of active detectors. A PADC track-etched solid-state detector with two types of radiators (for fast and slow neutrons) was used as a passive detector (Agafonov et al., 2013). The presence of this radiation component is detected in only a few experiments, and the production of neutrons in this field is still a subject of study.

The practical motivation for this work is threefold. First, workers operating high-voltage impulse generators may be exposed to ionizing radiation, and quantitative dosimetric data are required for occupational radiation protection assessments in accordance with ICRP Publication 103 (ICRP, 2007). Second, the use of passive detectors in an international intercomparison framework provides a validated methodology for dosimetry in pulsed, electromagnetically noisy environments — directly applicable to high-voltage test laboratories and analogous facilities. Third, controlled laboratory measurements, reproducible on demand, contribute benchmark data for theoretical models of lightning-related high-energy radiation phenomena such as TGFs and GRGs. Although laboratory discharge parameters differ fundamentally in scale from those of natural lightning, the underlying physical processes — bremsstrahlung emission from runaway electrons and potential photonuclear reactions — are the same, and the laboratory setting provides the only controllable environment in which their spatial and spectral properties can be systematically investigated.

Based on a literature review (Agafonov et al., 2013, 2017; Bassi et al., 2017; Dwyer et al., 2008; Nguyen et al., 2008; Rahman et al., 2008; Kochkin, 2014; Hettiarachchi et al., 2017b,a; Rahman et al., 2019) the aim of this international experiment was to measure the spatial radiation distribution along the entire length of a negative electric discharge with a wave type of 1.2/50 μs covering 180° around the discharge axis at a radius of 1 m using a selected combination of passive detectors.

This international comparative experiment follows up and expands on vertical measurements with TLDs along the main discharge axis (Kyselová et al., 2020) and horizontal measurements (Štěpánová et al., 2022) organized by Nuclear Physics Institute (NPI). The results of these previous experiments confirmed the presence of a photon/electron component and a neutron component of radiation for several measuring points at HVG.

These findings were leveraged in an international comparative experiment. The number of TLDs was increased to 120 per type and additional types of passive detectors were used for both photon/electron and neutron radiation. For better statistics, the number of negative

Table 2
Overview of lightning discharge experiments in a laboratory environment (part 2).

Study	Agafonov et al. (2017)	Bassi et al. (2017)	Hettiarachchi et al. (2017b)	Hettiarachchi et al. (2017a)	Rahman et al. (2019)	
Generator type	HVG	HVG	Marx generator	Marx generator	Marx generator	Marx generator
Voltage [MV]	1	0.11–1.1	0.95	0.95	0.8	0.8
Polarity	not specified	negative	negative	negative	negative	negative
Wave type [μs]	not specified	1.2/50	1.2/50	1.2/50	250/2500	250/2500
Electrode gap [m]	0.45–0.75	0.3–3	0.95	0.95	0.35	0.35 and 0.46
Electrode shape [–]	hemispheres, hemisphere (anode) and needle (cathode)	not specified	rod (cathode)-sphere (anode)	rod (cathode)-sphere (anode)	spherical	rod-plane (grounded)
Electrode material [–]	hemisphere: stainless steel, needle: TiN-coated carbon steel	not specified	rod: brass, spheres: chromium coating copper	rod: brass, spheres: chromium coating copper	chromium coating copper	rod: brass, plane: not specified
Electrode diameter [cm]	hemisphere: 0.8 and 0.9, needle: 0.06	not specified	rod: 0.1, sphere: 2.1, 6.3, 12	rod: 0.1, sphere: 2.1	12	rod: 0.1, sphere: 12
Discharge orientation	horizontal	horizontal	vertical	vertical	vertical/horizontal	vertical
Detectors	^{3}He proportional detector with paraffin moderator and plastic scintillator	TLD (LiF)	NaI(Tl) scintillator with PMT	NaI(Tl) scintillator with PMT	NaI scintillator (7.6 × 7.6 cm) with PMT, plastic scintillator (36 × 25 × 1 cm) with PMT	NaI scintillator (7.6 × 7.6 cm) with PMT, plastic scintillator (36 × 25 × 1 cm) with PMT
Distance of the detector from the discharge [m]	0.47–0.9 (plastic scintillator), 0.7 (^{3}He detector)	1–5	1.05	1.05	1.2 and 1.45 and 2.3	1.2 and 1.45 and 2.3
Detector shielding [–]	only plastic scintillators	no	yes	yes, only in some cases	yes	yes
Shielding material [m]	lead or aluminum	–	aluminum	copper	aluminum and lead	aluminum and lead
Shielding thickness [mm]	lead: 100 or 6, aluminum: 0.05	–	3.2	0.3 to 2.4	aluminum: not specified, lead: 32	aluminum: not specified, lead: 32
Number of discharges [–]	1261 (usual discharge), 116 (interrupted discharge)	4600	15 for each sphere	135	15 for vertical and 15 for horizontal	15 (7 for 0.35 m and 8 for 0.45 m)
Gamma/X-ray detection [–]	yes	yes	yes	yes	yes	yes
Neutron detection [–]	yes	not measured	not measured	not measured	not measured	not measured

discharges was also increased from 400 to 1000. The main differences of these experiments are shown in Table 3.

Five partners provided detectors and their evaluation for this experiment – NPI Czechia, Politecnico di Milano (POLIMI) Italy, Authority for Nuclear Safety and Radiation Protection (ANVS) France, National Centre for Nuclear Research (NCBJ) Poland, Research Centre Řež s.r.o. (CV) Czechia. Independent evaluation of the detectors ensured minimization of systematic error and robustness of the obtained results.

2. Materials and methods

2.1. High voltage impulse generator

A HVG SGDelta from Haefely was used for the experimental work, with a nominal voltage of 1000 kV, an energy of 100 kJ and generating pulses of the shape 1.2/50 μs with both polarities.

The generator setup was for 1000 consecutive negative discharges with voltage amplitude 900 kV, waveform like a standardized atmospheric pulse of 1.2/50 μs, discharge energy 80 kJ and electrodes 1 m apart. The HVG settings were the same as in previous experiments (Kyselová et al., 2020; Štěpánová et al., 2022). Only the number of negative discharges has been increased by 600 pulses, to decrease statistical errors.

2.2. Passive detectors

The passive radiation systems shown in Fig. 1 and listed in Table 4 were chosen to eliminate the influence of the electromagnetic field of the impulse generator and the discharge itself.

Based on previous experiments (Kyselová et al., 2020; Štěpánová et al., 2022), the following TLDs were specifically selected: $CaSO_4$:Dy detectors, three types of LiF:Mg:Ti (MTS-6/TLD-600, MTS-7/TLD-700, MTS-N/TLD-100). This combination was selected with regard to the expected detection of photon and neutron components.

Based on the different ratio of ^{6}Li and ^{7}Li, the detection of the thermal neutron component can be distinguished from the photon/electron radiation. All three types of detectors have the same response to the photon/electron component of the radiation (Obryk et al., 2008).

The difference in response between MTS-6/MTS-N (TLD-600/TLD-100) and MTS-7 (TLD-700) is quantified for the thermal neutron component as the gamma equivalent dose for neutrons (Stolarczyk et al., 2018). Their response to dose is linear from 50 μGy up to 5 Gy, the detection threshold is 10 μGy and thermal fading is 5% annually (TLD, 2026).

The $CaSO_4$:Dy type TLD is suitable for detecting the photon/electron component of radiation, to which it is approximately 30× more sensitive than the LiF:Mg:Ti type. Its response to dose is linear for absorbed dose in 10 μGy to 10 Gy, thermal fading is 7%–30% per six months (McKeever, 1985).

For each TLD, the conversion factor to translate the remeasured signal to air kerma was obtained separately, using calibration irradiation. This value was then converted to the absorbed dose in water.

For better statistics, their number was increased to 120 detectors per type. In previous measurements, a maximum of 40 detectors per type were used. The TLDs were placed in the same 3D printed holder as in Štěpánová et al. (2022).

Bubble detectors BD-PND (Bubble Detector – Personal Neutron Dosimeter, manufactured by Bubble Technology Industries) were also used, providing an immediate visible response to the measured dose

Table 3
Overview of the lightning discharge experiments in a laboratory environment organized by NPI.

Experiment	I	II	III
Article	Kyselová et al. (2020)	Štěpánová et al. (2022)	–
Experimental setup	horizontal	vertical	covering 180° around the discharge
Generator type	HVG	HVG	HVG
Voltage [MV]	0.9	0.9	0.9
Polarity	negative	negative	negative
Wave type [μs]	1.2/50	1.2/50	1.2/50
Electrode gap [m]	1	1	1
Electrode shape [–]	tip-plane	tip-plane	tip-plane
Discharge orientation	vertical	vertical	vertical
Detectors	TLD (MTS-6, MTS-7, MTS-N and $CaSO_4$:Dy	TLD (MTS-6, MTS-7, MTS-N and $CaSO_4$:Dy	TLD (MTS-6, MTS-7, MTS-N and $CaSO_4$:Dy, 600, 700, 100), RPL GD351 dosimeter, Bubble detectors BD-PND, Passive rem counter, PADC-based passive neutron spectrometer, gold foil, indium foil)
Number of TLDs	239	411	1180
Distance of the detector from the discharge [m]	0 (electrodes), 0.25, 0.5, 0.75, 1	0 (electrodes) and 1	0 (electrodes) and 1 (covering 180°)
Energy [kJ]	80	80	80
Number of discharge [–]	400	400	1000
Photon/electron detection [–]	yes	yes	yes
Neutron detection [–]	yes	yes	yes

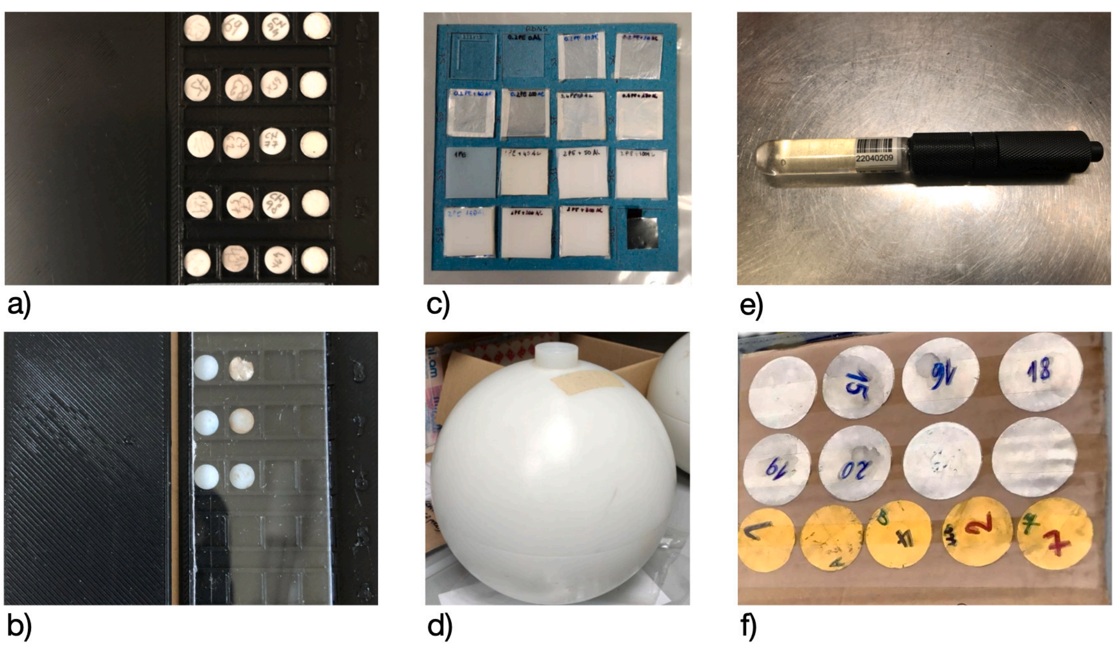

Fig. 1. The passive radiation systems (a) TLDs ($CaSO_4$:Dy, MTS-6/600, MTS-7/700 and MTS-N/100), (b) RPL GD351 dosimeters, (c) PADC-based passive neutron spectrometer, (d) passive rem counter, (e) bubble detectors BD-PND, (f) golden and indium foils.

of fast neutron radiation. The advantage of this type of detector is its insensitivity to photon/electron radiation. The energy range of this type of detector is from 200 keV to 15 MeV with a sensitivity of 1.9–3.7 bubbles/μSv. Specifically, bubble detectors with a sensitivity of 2.1–2.4 bubbles/μSv were used. The number of bubbles allows direct measurement of tissue equivalent neutron dose (Bubble, 2025).

The PADC-based passive neutron spectrometer contains 16 PADC detectors coupled to layers of aluminum and polyethylene with different thickness (Caresana et al., 2010, 2012). The detection limit of this neutron spectrometer in terms of neutron ambient dose equivalent is approximately 100 μSv. The detector signal value for HVG was compared to the detector signal value for background.

The passive rem counter is based on 2 PADC detectors coupled to ^{10}B-enriched converters for the detection of thermal neutrons (Agosteo et al., 2010; Caresana et al., 2014). It is shaped as a 25 cm diameter sphere made of polyethylene with an inner lead shell, to extend the response to neutron energies up to about 1 GeV. The advantage of this passive system based on PADC is that it is completely blind to photon dose. The detection limit of this detector in ambient dose equivalent from neutrons is about 10 μSv. The signal value from the passive rem counter located at the HVG was compared with the signal value of the background detector.

The radiophotoluminescence (RPL) GD351 dosimeter is a passive dosimeter based on a rod (diameter 1.5 mm and length 8.5 mm) of silver-activated phosphate glass inside a holder with a built-in Sn filter (0.75 mm) to improve the dosimeter's response to low-energy photons. The Low energy photon can be measured down to 15 keV, the relative response to neutrons is considered lower than 3%. The dynamic range is 0.05 mGy to 10 Gy (Zorloni et al., 2020; Yamamoto et al., 2011).

Table 4
The passive radiation systems.

Detector type	Quantity	Detection threshold	Detection	
			Gamma/X-ray	Neutrons
TLDs $CaSO_4$:Dy	Absorbed dose	1 μGy	yes	no
TLDs MTS-6/600	Absorbed dose	10 μGy	yes	yes (thermal)
TLDs MTS-7/700	Absorbed dose	10 μGy	yes	no
TLDs MTS-N/100	Absorbed dose	10 μGy	yes	yes (thermal)
RPL GD351 dosimeters	Air kerma	50 μGy	yes	no
Gold foils	Activity	0.01 Bq	yes	yes (thermal and fast)
Indium foils	Activity	0.01 Bq	yes	yes (thermal)
Bubble detectors BD-PND	Tissue-equivalent neutron dose	0.4–0.5 μSv	no	yes (fast)
Passive rem counter	Ambient dose equivalent	10 μSv	no	yes
PADC-based passive neutron spectrometer	Ambient dose equivalent	100 μSv	no	yes

Table 5
Detector placement in the laboratory setup of the experiment. Height h denotes vertical distance from the grounding electrode and θ the angle in horizontal plane.

Pos.	θ [°]	Detector type	Pieces for each type	h [cm]	Institute
1	0	TLDs ($CaSO_4$:Dy, MTS-6, MTS-7, MTS-N)	4 × 100	0–100	NPI
2	30	Gold foil	5	100	CV
		Indium foil	8	100	CV
3	60	Bubble detectors BD-PND	4	100	ANVS
4	90	TLDs (MTS-6, MTS-7, MTS-N)	3 × 80	21–100	NCBJ
		RPL GD351 dosimeter	30	1–30	ANVS
5	120	Passive rem counter	1	100	POLIMI
6	150	PADC-based passive neutron spectrometer	16	100	POLIMI
7	180	TLDs (600, 700, 100)	3 × 100	0–100	POLIMI
		TLDs ($CaSO_4$:Dy, MTS-6, MTS-7, MTS-N)	4 × 20		NPI
Backgr.	–	TLDs (MTS-6, MTS-7, MTS-N)	3 × 20	–	NCBJ
		RPL GD351 dosimeter	10		ANVS
		PADC	13		POLIMI
		TLDs (600, 700, 100)	3 × 20		POLIMI

Passive detectors in the form of foils are based on activation energy in the material for the detection of the neutron field. The gold activation foil allows for the determination of activities from neutrons as well as from beta and gamma radiation. The detection of thermal neutrons is determined based on the reaction $^{197}Au(n,\gamma)^{198}Au$ with a half-life of the resulting radionuclide of 2.69 d. The detection of fast neutrons is based on the reaction $^{197}Au(n,2n)^{196}Au$ with a half-life of the resulting radionuclide of 6.18 d and a threshold energy of 8.6 MeV. Neutron detection using activation analysis in indium foils is based on reactions $^{115}In(n,\gamma)^{116m}In$ with a half-life of the resulting radionuclide of 54.12 min. The activity of the activation detectors was determined within 4 h of the end of the experiment. The samples were evaluated using an HPGe detector.

The radiation field of the HVG was measured covering 180° around the discharge axis at a radius of 1 m using selected passive detectors in shown Table 5 and Fig. 2.

The background sets corresponding to the various detector types used in the experiment were stored in the high-voltage generator building, in a room adjacent to the one hosting the lightning generator during the experimental campaign. At all other times between preparation and evaluation, all detectors were stored and transported together.

3. Results

A statistically significant increase in absorbed dose/kerma compared to background values occurred only for passive TLDs, which were placed at positions 1, 4 and 7 at a height of 1 cm to 100 cm along the entire length of the negative electrical discharge.

The photon/electron radiation component occurred most often in the second half of the discharge at a height of 49–76 cm from the ground electrode. The maximum absorbed dose value of 1.2 ± 0.4 mGy was detected in the height range 24 cm to 31 cm using the MTS-7 for position 4.

A statistically significant increase in the neutron component of radiation was noted at heights of 21–27 cm and 95–100 cm with a maximum gamma-equivalent neutron dose of 6.9 ± 1.2 mGy at the height of 25 cm for position 1. These values have been calculated as the differences between the results of the MTS-N and MTS-7 TLDs. The uncertainty of the absorbed dose value was calculated as the pooled standard deviation for background values and values at HVG for a given TLD type at confidence level $k = 1$.

For TLDs and RPL GD351 dosimeters, the correction for the background was done by subtracting the mean dose of the respective type of the corresponding background measurement set. The results of absorbed dose/air kerma for a specific height from the ground electrode are given in Table 6. A two-sample t-test was employed to assess statistically significant differences between the mean absorbed dose/air kerma value given by the moving average for 5 (h to $h+4$, where h is the height (cm) from the ground electrode at the HVG) measurement position (μ_1) and the mean absorbed dose/air kerma in the background measurement set (μ_2). The zero hypothesis $H_0 : \mu_1 = \mu_2$ and the alternative hypothesis $H_1 : \mu_1 > \mu_2$ were tested, with the statistical significance level $\alpha = 0.05$.

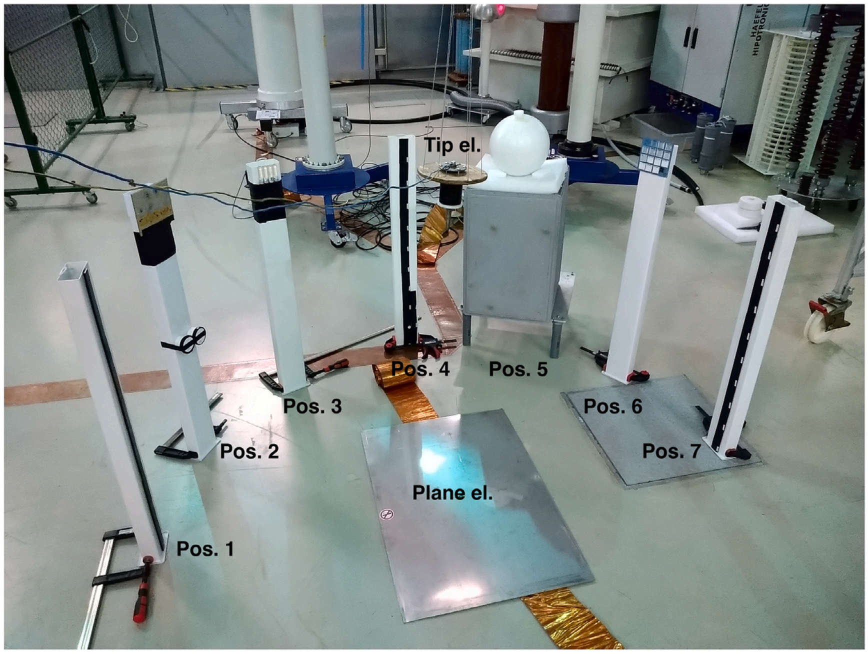

Fig. 2. Laboratory setup of experiment and position of each passive detectors.

This result was not confirmed by the passive rem counter and the PADC spectrometer that reported ambient dose equivalent comparable with the background.

4. Discussion

Although seven types of passive detectors were used during the measurement campaign to detect neutron and photon/electron of radiation components, a statistically significant increase in the measured quantity in the generator field compared to background values was recorded only with TLDs. The chosen combination of TLDs is sensitive to both radiation components and was distributed throughout the negative pulse discharge.

Unlike TLDs, the PADC-based rem counter, PADC based passive spectrometer, bubble detectors BD-PND are sensitive only to the neutron component of the radiation and were placed at a discharge height of 100 cm. The neutrons were only recorded by bubble detectors, but there was no statistically significant increase in the dose. The maximum gamma-equivalent neutron dose detected by TLDs at height of 96 cm was 1.6 ± 1.2 mGy for position 1.

For the detection of the neutron radiation component of a HVG using a gold foil activation detector, the threshold energy is 8.6 MeV for fast neutrons and with a resonance energy of 4.9 eV for thermal neutrons. In addition, the indium nuclide formed during the activation reaction has a very short half-life of only 54.12 min. Although the activation detectors were evaluated within 4 h of the end of the experiment, this short half-life could have influenced the result.

The RPL GD351 dosimeters were placed at a height of 1 cm to 30 cm from the ground electrode at position 4, where the maximum statistically significant absorbed dose for the photon/electron component was 1.2 ± 0.4 mGy detected by MTS-7 at the height of 25 cm. The RPL GD351 dosimeter recorded an increased air kerma value compared to the background at a height of 22 cm to 24 cm with a maximum value of 0.72 ± 0.05 mGy, but it was not statistically significant.

The absorbed dose values determined by MTS-6 at Position 1 are substantially higher than those determined by MTS-N at this position for several heights, and some individual readings (e.g. 18.7 mGy at h = 36 cm, 17.1 mGy at h = 26 cm) are among the largest single-detector values in the entire dataset. Despite this, the MTS-6 results were not classified as statistically significant based on the two-sample t-test with a 5-point moving average. This occurred because the elevated MTS-6 readings appear as isolated high values dispersed among near-background readings, resulting in a large variance within any given 5-point window. The mean of such a window therefore does not exceed the significance threshold ($\alpha = 0.05$), even when individual values are far above background. This pattern is in contrast to MTS-N at heights 21–27 cm and 95–100 cm, where elevated readings are more consistently clustered. The physical origin of the sporadic high MTS-6 values is not conclusively established; possible explanations include direct energy deposition by secondary charged particles or local geometric effects near the discharge axis. This behavior will be the subject of further dedicated investigation.

5. Conclusion

In this international comparative experiment, the radiation field was measured covering 180° around the discharge axis at a radius of 1 m using passive detectors. The settings of the pulsed HVG were the same as in the previous experiments (Kyselová et al., 2020; Štěpánová et al., 2022). In this experiment, the number of negative discharges was increased from 400 to 1000 pulses, for better statistics.

The photon/electron and neutron components of the radiation were confirmed using passive TLDs. The photon/electron radiation component occurred the most often in the second half of the discharge at a height of 49–76 cm from the ground electrode. The maximum statistically significant absorbed dose value of 1.2 ± 0.4 mGy was detected at height range 24–31 cm using MTS-7 for position 4.

A statistically significant increase in the neutron component of radiation was registered limited to MTS-N TLDs at heights of 21–27 cm and 95–100 cm, with a maximum gamma-equivalent neutron dose of 6.9 ± 1.2 mGy at the height of 25 cm in position 1. Since the neutron component was registered by only a single, specific type of detectors and no established physical model or mechanism currently exists to explain the generation of neutrons during atmospheric discharges in air, the results of this study are not sufficient to confirm the actual presence of neutrons. Still, the present work can pave the way for further investigations in this sense, particularly focusing on the regions near the electrodes.

Table 6
Absorbed dose [mGy] determined by TLDs and air kerma [mGy] determined by RPL GD351 dosimeter net of background value for a specific height h [cm] from the ground electrode at HVG.

h [cm]	Position 1: NPI				Position 4: NCBJ and ANVS				Position 7: POLIMI		
	MTS-6	MTS-7	MTS-N	$CaSO_4$	MTS-6	MTS-7	MTS-N	GD351	TLD-600	TLD-700	TLD-100
100	*	0.2	0.2	0.04	*	0.0	0.09		0.04	0.04	*
99	*	0.5	0.9	*	0.0	0.0	0.12		0.07	0.07	0.007
98	*	0.3	0.0	0.01	0.0	0.0	0.03		0.02	0.03	0.018
97	*	0.2	0.1	*	0.0	0.0	0.03		0.03	0.04	0.004
96	*	*	1.6	0.00	0.0	*	*		0.03	0.03	0.012
95	*	0.6	0.1	0.01	*	0.0	*		0.00	0.00	0.009
94	14.4	0.0	*	0.02	*	1.4	*		0.01	0.01	*
93	*	0.3	0.0	0.00	*	*	*		0.02	0.02	*
92	*	0.5	0.0	0.03	*	0.0	*		0.01	0.02	0.008
91	*	*	0.4	0.01	*	*	*		*	0.03	0.007
90	*	0.2	0.1	*	*	*	*		0.01	0.00	0.010
89	10.4	0.3	0.5	0.00	0.3	*	*		0.01	0.00	0.010
88	*	*	*	0.03	0.3	0.2	0.33		0.00	0.01	*
87	*	0.6	0.3	0.03	0.1	0.2	0.14		0.01	0.01	0.003
86	*	*	0.5	*	0.3	0.2	0.11		0.03	0.00	0.015
85	*	*	0.3	0.03	0.3	0.0	0.17		0.00	0.01	0.030
84	9.6	*	5.8	*	0.3	0.1	0.22		*	0.03	0.005
83	11.4	4.4	*	0.06	0.2	0.2	0.14		0.00	*	0.003
82	11.3	0.0	0.1	*	*	0.0	0.16		0.01	*	0.006
81	*	*	*	0.04	0.1	*	0.01		0.00	*	0.006
80	*	*	0.2	0.02	0.1	0.2	0.12		0.01	0.01	*
79	*	*	0.6	0.01	0.1	0.0	0.10		0.00	0.01	*
78	*	0.2	*	*	0.0	*	0.02		*	0.00	0.032
77	*	*	0.2	0.00	0.1	0.1	0.01		0.01	0.00	0.000
76	*	*	0.6	0.02	0.0	0.0	*		0.00	*	0.000
75	*	0.3	0.1	*	*	0.0	0.10		0.05	0.02	0.015
74	*	0.2	0.7	0.02	*	*	*		0.03	0.04	*
73	*	0.2	0.2	*	*	*	*		0.04	0.01	0.004
72	*	*	0.1	0.02	0.1	0.0	0.07		0.00	0.15	0.007
71	11.9	*	0.0	0.00	0.2	0.0	0.10		0.01	0.02	0.018
70	*	0.2	0.0	0.00	0.4	0.3	0.27		0.00	*	0.002
69	*	*	0.1	0.00	0.1	0.2	0.15		0.01	0.02	0.008
68	13.6	*	0.0	0.03	0.2	0.2	0.12		*	0.02	0.004
67	*	0.3	0.2	*	0.5	0.3	0.15		*	*	*
66	9.0	*	*	*	0.3	0.2	0.25		0.00	*	0.002
65	7.0	*	0.3	*	0.3	0.3	0.45		*	*	0.003
64	*	0.2	0.4	0.04	0.2	0.2	0.09		0.00	0.00	0.003
63	6.5	0.2	0.5	0.03	0.2	0.3	0.35		*	*	0.004
62	*	0.0	0.2	*	0.5	0.3	0.35		*	*	0.007
61	*	*	0.2	0.00	0.3	0.3	0.29		*	0.01	0.028
60	*	0.1	0.1	0.04	0.3	0.1	0.15		*	*	0.000
59	*	*	0.2	0.09	0.1	0.2	0.10		0.00	*	0.015
58	*	0.1	0.1	*	0.0	0.1	*		*	*	*
57	*	0.3	*	0.02	*	0.0	0.06		*	0.01	0.005
56	*	*	0.1	0.02	0.1	0.0	*		0.00	*	0.009
55	*	*	0.0	0.01	*	0.0	*		*	0.01	0.006
54	*	*	0.4	0.00	0.3	0.1	*		*	0.04	0.052
53	12.3	0.2	0.0	0.01	0.2	0.2	0.16		0.00	0.03	0.003
52	*	*	0.4	0.02	0.4	0.4	0.43		0.01	0.04	0.066
51	*	*	0.3	*	0.2	0.1	0.32		0.03	0.03	0.074
50	11.3	*	0.4	0.05	0.1	0.0	0.04		0.00	0.01	0.034
49	*	0.0	*	*	0.0	0.0	0.02		0.01	0.00	*
48	9.3	*	0.2	0.00	0.0	0.0	0.09		0.02	0.00	0.008
47	10.2	*	0.1	0.03	*	0.0	0.03		0.02	0.01	*
46	*	*	*	0.00	*	*	*		0.00	0.00	*
45	*	*	*	0.01		*	*		0.00	0.00	*
44	*	*	0.0	*	*	*	*		*	0.00	*
43	*	0.0	0.3	0.00	*	0.0	*		0.13	*	0.003
42	8.7	0.0	0.3	*	*	*	*		*	0.01	0.000
41	*	*	0.0	0.00	*	*	*		*	*	*
40	*	0.0	0.0	0.00	*	0.0	*		*	*	*
39	*	0.0	0.3	0.02	*	0.0	*		*	0.00	*
38	11.3	*	*	*	*	*	*		*	*	0.004
37	*	0.1	0.0	*	*	*	*		*	*	*
36	18.7	*	0.2	*	0.0	0.1	0.08		0.00	*	0.010
35	*	*	0.1	*	0.0	2.4	0.04		*	*	*
34	*	0.3	*	*	0.0	0.0	0.06		*	*	0.007
33	*	*	0.1	0.04	0.0	0.0	0.08		*	0.00	0.000
32	*	*	0.4	*	0.0	*	0.04		*	0.00	0.007
31	*	0.7	0.6	*	0.0	0.0	*		0.00	0.00	*
30	*	0.2	0.5	*	0.0	0.0	*	0.00	*	0.01	*

h [cm]	Position 1: NPI				Position 4: NCBJ and ANVS				Position 7: POLIMI		
	MTS-6	MTS-7	MTS-N	$CaSO_4$	MTS-6	MTS-7	MTS-N	GD351	TLD-600	TLD-700	TLD-100
29	5.3	0.4	*	*		0.1	*	*	*	0.00	*
28	*	*	*	0.01	*	0.6	*	*	*	0.01	*
27	*	*	0.5	*	1.3	1.2	*	*	0.01	0.02	0.000
26	17.1	0.0	*	*	*	*	*	*	*	0.02	0.004
25	*	*	6.9	*	*	*	*	*	0.00	0.00	0.010
24	1.0	*	*	0.00	*	0.1	*	0.07	0.00	*	*
23	5.5	*	0.7	0.00	*	*	*	0.00	*	*	*
22	*	*	*	*	*	*	*	0.07	*	*	*
21	10.7	*	0.4	0.01	*	*	*	*	0.00	*	*
20	*	*	0.5	0.04				*	*	*	*
19	*	0.3	*	0.02				*	*	*	*
18	*	*	*	0.00				*	*	*	0.010
17	*	*	*	0.05				*	*	0.00	0.003
16	6.9	0.1	*	0.04				*	*	*	*
15	*	*	*	0.03				*	0.01	*	0.008
14	*	*	0.1	0.03				*	0.00	*	*
13	*	0.0	0.0	*				*	0.00	*	*
12	*	0.5	*	0.00				*	*	*	0.007
11	*	*	*	*				*	*	0.00	*
10	*	*	*	*				*	0.00	*	*
9	*	*	0.0	*				*	0.00	*	*
8	13.5	*	0.1	0.00				*	*	*	0.003
7	*	*	*	*				*	*	*	*
6	6.3	*	0.3	0.06				*	*	*	0.060
5	*	*	*	*				*	0.00	*	0.012
4	8.0	*	1.1	0.01				*	*	*	0.013
3	*	*	0.2	0.05				*	*	0.00	0.006
2	15.2	*	0.1	0.04				*	*	0.02	0.014
1	*	*	*	*				*	0.05	0.04	0.008

* Absorbed dose/air kerma value is lower than the average background value. The red area represents statistically significant differences between the mean absorbed dose/air kerma value given by the moving average for 5 measurement position (h to $h+4$, where h is the height [cm] from the ground electrode at the HVG) and the mean absorbed dose/air kerma in the background measurement set.

One limitation of the present intercomparison design is that each participating institution placed their detectors at a different azimuthal position, making it impossible to separate differences arising from detector characteristics from those due to the known spatial inhomogeneity of the radiation field (Agafonov et al., 2019; Parkevich et al., 2024). For future experiments, we recommend that at least a subset of detectors from different participants be co-located at the same positions — particularly at heights where the radiation signal is expected to be strongest based on the present results (around 24–31 cm and 95–100 cm). In addition, placing a common set of reference TLD (insensitive to neutrons, such as MTS-7) from a single institution at all angular positions would provide a direct map of field inhomogeneity and allow cross-calibration across participant detector types.

CRediT authorship contribution statement

D. Štěpánová: Writing – review & editing, Writing – original draft, Validation, Methodology, Investigation, Formal analysis, Data curation, Conceptualization. **J. Mikeš:** Writing – review & editing, Writing – original draft, Validation, Project administration, Methodology, Investigation, Funding acquisition, Formal analysis, Conceptualization. **V. Štěpán:** Writing – review & editing, Writing – original draft, Methodology, Investigation, Formal analysis, Conceptualization. **I. Ambrožová:** Validation, Investigation. **M. Bolzonella:** Validation, Investigation. **M. Caresana:** Validation, Investigation. **L. Garlati:** Validation, Investigation. **M. Košťál:** Validation, Investigation. **M. Krbal:** Validation, Investigation. **M. Lužová:** Validation, Investigation. **A. Mele:** Validation, Investigation. **F. Trompier:** Validation, Investigation. **M. Wiliński:** Validation, Investigation. **O. Ploc:** Validation, Investigation.

Funding

This work was supported by CTU internal project SGS23/070/OHK5/1T/13 and BUT specific project FEKT-S-23-8403. The authors acknowledge the EURADOS Working Group 11 (WG11) High Energy Radiation Fields for providing the collaborative framework that enabled this intercomparison study. The experiment benefited from the coordinated participation of WG11 members, including the contribution of passive dosimeters and expert input to the experimental design and data interpretation.

Declaration of competing interest

The authors declare that they have no known competing financial interests or personal relationships that could have appeared to influence the work reported in this paper.

Data availability

Data will be made available on request.

References

Agafonov, A.V., Bagulya, A.V., Dalkarov, O.D., Negodaev, M.A., Oginov, A.V., Rusetskiy, A.S., Ryabov, V.A., Shpakov, K.V., 2013. Observation of neutron bursts produced by laboratory high-voltage atmospheric discharge. Phys. Rev. Lett. 111 (11), http://dx.doi.org/10.1103/PhysRevLett.111.115003.

Agafonov, A.V., Bogachenkov, V.A., Chubenko, A.P., Oginov, A.V., Rodionov, A.A., Rusetskiy, A.S., Ryabov, V.A., Shepetov, A.L., Shpakov, K.V., 2017. Observation of hard radiations in a laboratory atmospheric high-voltage discharge. J. Phys. D: Appl. Phys. 50 (16), 165202. http://dx.doi.org/10.1088/1361-6463/aa5dba.

Agafonov, A.V., Oginov, A.V., Rodionov, A.A., Ryabov, V.A., Shpakov, K.V., 2019. Anisotropy in hard bremsstrahlung from a high-voltage laboratory simulation of an atmospheric discharge. Plasma Sources Sci. Technol. 28, 095014. http://dx.doi.org/10.1088/1361-6595/ab3c79.

Agosteo, S., Caresana, M., Ferrarini, M., Silari, M., 2010. A dual-detector extended range rem-counter. Radiat. Meas. 45 (10), 1217–1219. http://dx.doi.org/10.1016/j.radmeas.2010.05.002.

Bassi, W., Bottaro, M., Viana, V., Tatizawa, H., 2017. One year of X-Ray dosimetry in a high voltage laboratory. Electr. Power Syst. Res. 145, 83–88. http://dx.doi.org/10.1016/j.epsr.2016.12.022.

Bubble, 2025. Bubble Detectors Neutron Dosimeters. Bubble Technology Industries, URL https://www.bubbletech.ca/wp-content/uploads/2022/04/BTI_BUBBLE_General_2025-Apr-11-pdf.

Caresana, M., Ferrarini, M., Parravicini, A., Sashala Naik, A., 2014. Calibration of a passive rem counter with monoenergetic neutrons. Radiat. Meas. 71, 498–501. http://dx.doi.org/10.1016/j.radmeas.2014.07.019.

Caresana, M., Ferrarini, M., Pola, A., Agosteo, S., Campi, F., Porta, A., 2010. Study of a radiator degrader CR39 based neutron spectrometer. Nucl. Instruments Methods Phys. Res. Sect. A: Accel. Spectrometers, Detect. Assoc. Equip. 620 (2–3), 368–374. http://dx.doi.org/10.1016/j.nima.2010.03.105.

Caresana, M., Ferrarini, M., Porta, A., Campi, F., 2012. Performance evaluation of a radiator degrader CR39 based neutron spectrometer. Nucl. Instruments Methods Phys. Res. Sect. A: Accel. Spectrometers, Detect. Assoc. Equip. 680, 155–160. http://dx.doi.org/10.1016/j.nima.2012.02.050.

Dwyer, J.R., 2008. Source mechanisms of terrestrial Gamma-ray flashes. J. Geophys. Res.: Atmospheres 113 (D10), http://dx.doi.org/10.1029/2007JD009248.

Dwyer, J.R., Saleh, Z., Rassoul, H.K., Concha, D., Rahman, M., Cooray, V., Jerauld, J., Uman, M.A., Rakov, V.A., 2008. A study of X-ray emission from laboratory sparks in air at atmospheric pressure. J. Geophys. Res. 113 (D23), D23207. http://dx.doi.org/10.1029/2008JD010315.

Hettiarachchi, P., Cooray, V., Rahman, M., Dwyer, J., 2017a. Energy distribution of X-rays produced by meter-long negative discharges in air. Atmosphere 8, http://dx.doi.org/10.3390/atmos8120244.

Hettiarachchi, P., Rahman, M., Cooray, V., Dwyer, J., 2017b. X-rays from negative laboratory sparks in air: Influence of the anode geometry. J. Atmos. Sol.-Terr. Phys. 154, 190–194. http://dx.doi.org/10.1016/j.jastp.2016.07.012.

ICRP, 2007. The 2007 Recommendations of the International Commission on Radiological Protection. ICRP publication 103. Ann. ICRP 37 (2–4).

Kochkin, P., 2014. Understanding Lightning: Experiments on Meter Long Discharges and Their x-Rays (Doctoral thesis). Technische Universiteit Eindhoven, http://dx.doi.org/10.6100/IR783261.

Kovář, P., Puričer, P., Mikeš, J., 2023. Study of the applicability of radio signals emitted by lightning for long-range navigation. J. Navig. 76 (6), 641–652. http://dx.doi.org/10.1017/s0373463324000031.

Kyselová, D., Mikeš, J., Štěpán, V., Ambrožová, I., Benton, E.R., Sommer, M., Krbal, M., Pelikán, L., Ploc, O., Reitz, G., 2020. Measurements of radiation induced by a spark discharge under laboratory conditions. Radiat. Meas. 137, 106420. http://dx.doi.org/10.1016/j.radmeas.2020.106420.

McKeever, S.W.S., 1985. Thermoluminescence of Solids, first ed. Cambridge University Press, http://dx.doi.org/10.1017/CBO9780511564994.

Nguyen, C.V., Deursen, A.P.J., Ebert, U., 2008. Multiple X-Ray bursts from long discharges in air. J. Phys. D: Appl. Phys. 41 (23), 234012. http://dx.doi.org/10.1088/0022-3727/41/23/234012.

Obryk, B., Bilski, P., Budzanowski, M., Fuerstner, M., Ilgner, C., Jaquenod, F., Olko, P., Puchalska, M., Vincke, H., 2008. The response of different types of TL lithium fluoride detectors to high-energy mixed radiation fields. Radiat. Meas. 43 (2–6), 1144–1148. http://dx.doi.org/10.1016/j.radmeas.2007.11.039.

Parkevich, E.V., Shpakov, K.V., Baidin, I.S., Rodionov, A.A., Khirianova, A.I., Bolotov, Y.K., Ryabov, V.A., 2024. Angular anisotropy of hard x rays produced by laboratory atmospheric discharges. J. Appl. Phys. 136, http://dx.doi.org/10.1063/5.0227554.

Rahman, M., Cooray, V., Ahmad, N.A., Nyberg, J., Rakov, V.A., Sharma, S., 2008. X rays from 80-cm long sparks in air. Geophys. Res. Lett. 35 (6), http://dx.doi.org/10.1029/2007GL032678.

Rahman, M., Hettiarachchi, P., Cooray, V., Dwyer, J., Rakov, V., Rassoul, H.K., 2019. X-rays from negative laboratory sparks in air: Influence of the anode geometry. Atmosphere 10, http://dx.doi.org/10.3390/atmos10040169.

Štěpánová, D., Mikeš, J., Štěpán, V., Krbal, M., Ploc, O., 2022. Vertical dosimetric measurement of electric discharge induced at lightning impulse voltage generator. Radiat. Prot. Dosim. 198 (9–11), 617–622. http://dx.doi.org/10.1093/rpd/ncac107.

Stolarczyk, L., Trinkl, S., Romero-Expósito, M., Mojżeszek, N., Ambrozova, I., Domingo, C., Davídková, M., Farah, J., Kłodowska, M., Knežević, Z., Liszka, M., Majer, M., Miljanić, S., Ploc, O., Schwarz, M., Harrison, R.M., Olko, P., 2018. Dose distribution of secondary radiation in a water phantom for a proton pencil beam—EURADOS WG9 intercomparison exercise. Phys. Med. Biol. 63 (8), 085017.

TLD, 2026, URL https://www.radcard.pl/download/detektory.pdf.

Yamamoto, T., Rosenfeld, A., Kron, T., d'Erico, F., Moscovitch, M., 2011. RPL dosimetry: Principles and applications. In: Concepts and Trends in Medical Radiation Dosimetry: Proceedings of SSD Summer School. pp. 217–230. http://dx.doi.org/10.1063/1.3576169.

Zorloni, G., Ambrožová, I., Carbonez, P., Caresana, M., Ebert, S., Olšovcová, V., Pitzschke, A., Ploc, O., Pozzi, F., Silari, M., Trompier, F., Trunecek, R., Zelenka, Z., 2020. Intercomparison of personal and ambient dosimeters in extremely high-dose-rate pulsed photon fields. Radiat. Phys. Chem. 172, 108764. http://dx.doi.org/10.1016/j.radphyschem.2020.108764.